

We are IntechOpen, the world's leading publisher of Open Access books Built by scientists, for scientists

6,900

Open access books available

185,000

International authors and editors

200M

Downloads

Our authors are among the

154

Countries delivered to

TOP 1%

most cited scientists

12.2%

Contributors from top 500 universities



WEB OF SCIENCE™

Selection of our books indexed in the Book Citation Index
in Web of Science™ Core Collection (BKCI)

Interested in publishing with us?
Contact book.department@intechopen.com

Numbers displayed above are based on latest data collected.
For more information visit www.intechopen.com



Synthesis and Characterization of Nanocomplexes by Green Chemistry and Their Applications in Different Fields

Rania H. Taha

Abstract

In this study, a convenient synthesis of a series of La(III) complexes (in nanoscales) with different organic ligands was prepared by green chemical method. The physicochemical properties of the nanocomplexes were obtained. The SEM and TEM techniques were used to confirm the nanosize and morphology. The cytotoxicity of the newly synthesized compounds was demonstrated and tested for their anticancer activity against common pathogenic organisms and against human epithelial colorectal adenocarcinoma cells (Caco2), Vero, and MCF-7 cells. By examining its pharmacological activity, we were able to identify new potent and selective anticancer agents. Also, the structures succeeded to affect and stop the growth of *Klebsiella pneumonia* strain, and the results revealed promising activity. In addition, an electrospinning technique was used for the fabrication of novel bio-medicated nanofibers which are applied for wound dressing as local chemotherapy for skin injuries.

Keywords: nanocomplexes, anticancer activity, Caco2, vero, MCF-7 cells, flow cytometry, electrospinning, wound dressing

1. Introduction

The Environmental Protection Agency defined the green chemistry or sustainable chemistry as “the production of chemical products and processes which have the ability to reduce or eliminate the use or generation of hazardous substances.” In recent years there is an expectation that chemists and chemical engineers should design greener and more sustainable chemical processes, and it was expected that this trend will continue to grow over the next few decades [1].

Studies on metal-based drugs offer promise in the fight against cancer, which is the main aim of the inorganic chemistry [2, 3].

The metal-based anticancer drugs are driven by the necessity to fill the gap in tumor chemotherapy in order to minimize the undesirable side effects and enlarge the spectrum of activity for more tumor types and metastatic cancers. The Schiff base structures play a key role in studying the mechanism of the transformation and racemization reaction in biological systems due to the similarity of their structures to the natural biological system [4–11].

Among various metal complexes, La(III) complexes have been intensively investigated due to their more physiological activities and lower toxicities after coordination with ligand, so, in recent years people have paid great interest to synthesis, DNA interaction, and anticancer activity of La(III) complexes [12–16].

Dressings play multimodal roles in wound healing process, such as preventing infections, absorbing exudates, and maintaining moisture, and thus are indispensable [17]. Electrospinning is the method to fabricate ultrafine fibers from polymer solution(s) or melt(s) with diameters ranging from nanometers to micrometers [18].

The obtained results revealed the successful implementation of the nanoparticle-nanofiber as a local wound dressing especially for skin injuries.

2. Experimental

2.1 Materials and reagents

In this study all chemicals used were of highest purity. Organic solvents such as ethyl alcohol and dimethylformamide (DMF) were spectroscopically pure from the British Drug House (BDH). The other materials were purchased from Sinopharm Chemical Reagent Co., Ltd. and used without further purification. In addition to the 5-bromosalicylaldehyde (Sigma-Aldrich), $\text{La}(\text{NO}_3)_3 \cdot 6\text{H}_2\text{O}$ (Merck) were also used.

2.2 Instrumentation

In open capillaries melting points ($^{\circ}\text{C}$, uncorrected) were determined on a Gallenkamp melting point apparatus (Sanyo Gallenkamp, Southborough, UK). In the Microanalytical Center, Cairo University (C, H, N, and S) were carried out. ^1H NMR spectra ($\text{DMSO}-d_6$) were measured at Bruker FT-400MHZ spectrophotometer. The IR spectra were recorded on a Perkin Elmer 437 IR spectrophotometer ($400\text{--}4000\text{ cm}^{-1}$) (KBr technique). Thermogravimetric analysis was performed using a Shimadzu TGA-50H with a flow rate of 20 ml min^{-1} . The UV-vis spectra were recorded on a Perkin Elmer Lambda 3B UV-vis spectrophotometer. X-ray diffraction were recorded at room temperature ($\sim 25^{\circ}\text{C}$) on Empyrean X-ray diffractometer equipped. The patterns were run with Cu target ($\text{CuK}\alpha$ radiation), and the tube operated at 45 kV and 30 mA. The size and morphology of the nanocomplexes were characterized with a scanning electron microscope (SEM) (Philips XL 30) with gold coating and TEM.

2.3 Cytotoxicity assay

Different concentrations of the nanometal complexes were tested for their cytotoxicity against Vero, Caco2, and MCF-7 cell lines using (MTT) Thiazolyl Blue Tetrazolium Bromide method according to [19, 20]. In brief, Vero, Caco2, and MCF-7 cells (10×10^3) were cultured in a 96-well plate overnight at 37°C , 5% CO_2 , and 88% humidity. The total volume of used DEMEM supplemented medium and the synthesized compound supernatant was $200\text{ }\mu\text{L}$ with final concentrations of 10, 20, 30, 40, 60, 80, and 100 mg/L . The plate was incubated at 37°C and 5% CO_2 for 3 days. After incubation, debris and dead cells were removed by washing three times with fresh medium. Twenty microliters of MTT solution (5 mg/mL of MTT in PBS buffer) was added to each well and shook for 5 min at 150 rpm to thoroughly mix the MTT into the media. The cells were incubated at 37°C and 5% CO_2 for 3–5 h to

metabolize MTT by viable cells. Two hundred microliter dimethyl sulfoxide (DMSO) was added to each well and shook again for 5 min at 150 rpm, and then the viability of the cells was calculated by measuring the optical density at 630 nm subtracted from optical density at 570 nm [21]. The percentage of viability cells was calculated by comparison with control cells (without adding the synthesized compounds to the cells) using the equation $(A)_{\text{test}} / (A)_{\text{control}} \times 100$.

2.4 Flow cytometry

To discriminate living cells from dead cells or for cell cycle analysis, propidium iodide (PI) can be used according to Léonce et al. [22]. This analysis is based on the stoichiometric binding of PI to intracellular DNA. At the end, cells were washed with PBS and collected by trypsinization. Cells were then resuspended in warm PBS and fixed with 4 ml ice-cold ethanol. Finally, in darkness, cells were stained with 0.5 ml of warm PI solution; 7 ml of PI solution consists of 0.35 ml of PI stock solution (1 mg/ml), 0.7 ml RNase A stock solution (1 mg/ml), and 6 ml of PBS and incubated in darkness for 30 minutes. The samples were kept on ice until flow cytometric analysis.

2.5 Preparation of (chitosan-La(III) nanocomplex) composite nanofibers

Chitosan (CS) was dissolved in 50% acetic acids at room temperature under moderate stirring for 12 h to form a homogeneous solution, and then the solution of La complex nanoparticles was quietly adding. The total solution was fixed to 3 wt.%. The solution was filled in a 20 ml NORM-JECT Luer Lock tip plastic syringe having an 18-gauge stainless steel needle with 90° blunt end. The electrospinning setup included a high voltage power supply, purchased from the NanoNC, Inc. (S. Korea), and a nanofiber collector of aluminum foil that covered a laboratory-produced roller with the diameter of 10 cm. The collector was placed at 10 cm tip-to-collector distance (TCD) [39].

2.6 Synthesis

2.6.1 Synthesis of complex nanoparticles by sonochemistry method (green chemistry)

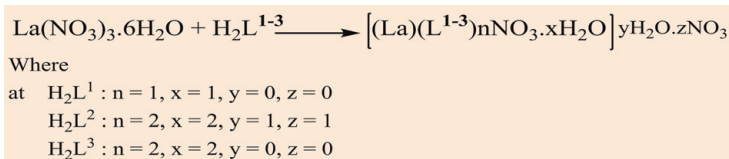
Ten milliliter of 0.1 M solution of $\text{La}(\text{NO}_3)_3 \cdot 6\text{H}_2\text{O}$ in ethanol was positioned in a high-density ultrasonic probe, operating at 24 kHz with a maximum power [23] output of 400 W. Ten milliliter of 0.1 M solution of $\text{N}'\text{-}((\text{E})\text{-}5\text{-bromo-}2\text{-hydroxybenzylidene})\text{-}6\text{-}(((\text{E})\text{-}5\text{-bromo-}2\text{-hydroxybenzylidene})\text{amino})\text{-}4\text{-oxo-}2\text{-thioxo-}1,2,3,4\text{-tetrahydrothieno}[3,2\text{-d}]\text{pyrimidine-}7\text{-carbohydrazide}$ H_2L^1 , $\text{N}\text{-}(2\text{-mercaptophenyl})\text{ benzamide}$ H_2L^2 , and $2\text{-}((2\text{-mercapto-phenyl})\text{ imino})\text{-}1,2\text{-diphenylethan-}1\text{-ol}$ H_2L^3 was added dropwise. The obtained precipitates were allowed to evaporate at room temperature to obtain the complex nanoparticle in powder form.

3. Results and discussion

3.1 Elemental analyses for nanometal complexes

In the present investigation, the analytical data of the prepared metal complexes suggest the structures as given in **Figure 6**. The physicochemical results of the newly synthesized compounds were presented in **Table 1**. The obtained results

were in good agreement with those calculated for the suggested formulae. The melting points were sharp, indicating the purity of the prepared nanometal complexes. The proposed formula of the nanometal complexes is according to the following general equations:



3.2 ^1H NMR spectra

The ^1H NMR spectra (Figure 1, Table 2) of the La (III) nanocomplex **1** showed a singlet peak at 8.00 ppm assigned to azomethine proton, in addition to the multiplet signals due to aromatic protons. It was found that the spectra of complex **2** display singlet peaks due to SH and NH groups at δ 3.5 and 5.4 ppm indicating the involvement of these groups in coordination with the metal atoms without deprotonation.

In addition to the ^1H NMR spectra of complex **3**, showed singlet peaks due to the O–H proton at 10.4 ppm and the S–H proton peak at 3.47 ppm. This analysis showed that the O–H and S–H groups share in the complexation a loss of their protons. Moreover, the spectra of the complexes showed multiplet signals at 6.99–7.48 ppm attributed to the aromatic protons for all complexes [24, 25].

Compd. code	(Empirical formula)	M.P. (°C)	Color (yield %)	(%) found (calcd.)				
				C	H	N	S	Δm^*
1	$[(\text{La})(\text{L}^1)(\text{NO}_3)(\text{H}_2\text{O})]$	<350	Faint orange (80.54)	29.90 (30.01)	1.32 (1.56)	9.92 (10.00)	7.58 (7.62)	20.51
2	$[\text{La}(\text{H}_2\text{L}^2)(\text{NO}_3)_2(\text{H}_2\text{O})_2]\text{NO}_3 \cdot \text{H}_2\text{O}$	110	Dark gray (85.49)	2.94 (3.06)	27.75 (27.87)	5.40 (5.71)	9.80 (10.00)	57.88
3	$[\text{La}(\text{H}_2\text{L}^3)(\text{NO}_3)_3 \cdot \text{H}_2\text{O}]$	165	Page (79.80)	2.83 (2.90)	36.54 (36.31)	4.55 (4.83)	8.33 (8.47)	3.39

* $\text{ohm}^{-1}\text{cm}^2\text{mol}^{-1}$

Table 1.
Elemental analysis and some physical measurements of La(III) nanocomplexes (**1–3**).

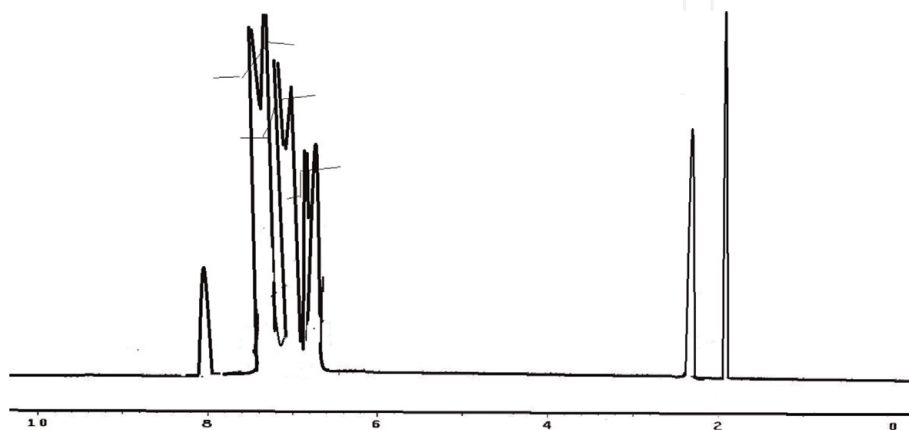


Figure 1.
 ^1H NMR data for La(III) diamagnetic complex (**1**).

Compd. no.	δ_{ph}	$\delta_{\text{CH=N}}$	δ_{SH}	δ_{NH}	δ_{OH}
1	6.39–8.46	8.00	–	–	–
2	6.99–7.48	–	3.5	5.4	–
3	7.00–8.00	–	3.47	–	10.4

Table 2.
¹H NMR data for La(III) nanocomplexes.

3.3 IR spectra and mode of bonding

In order to ascertain the mode of bonding, the IR spectrum of the free ligands was compared with those of their La complexes. By careful comparison of the spectra of the complexes with those of the free ligands, it was found that the band at 3430 cm^{-1} is found to be disappeared by complexation suggesting the involvement of OH groups of the phenolic groups in complex formation with their deprotonation. The bands due to NH and SH are shifted to higher or lower frequencies indicating the participation of –N and –S donors in the coordination, while the bands due to C=O are unchanged. The strong bands at 1622 and 1298 cm^{-1} due to $\nu_{\text{C=N}}$ and $\nu_{\text{C=O}}$ (azomethine and phenolic groups) are shifted to lower wave number 1609 – 1565 and 1280 – 1242 cm^{-1} , respectively, in metal complexes indicating the participation of nitrogen of azomethine and oxygen of phenolic group in complexation. The complexes showing also three bands at the range 1480 – 1400 , 1380 – 1350 , and 1170 – 1020 cm^{-1} indicate the unidentate coordination mode of the nitrate group. The curves also, showed that shift in the peaks of O–H, C–O, C–S groups (complex 3) due to their sharing in the complexation and that recorded by the M–O, and M–S peaks. All these results are in good agreement with the conductance data. Another evidence for the coordination is the observance of new bands in the far IR region at 570 – 505 , 520 – 440 , and 432 – 524 cm^{-1} which may be due to $\nu_{\text{M=O}}$, $\nu_{\text{M=N}}$ and $\nu_{\text{M=S}}$, respectively, that are not observed in the spectrum of the free ligands [26, 27].

3.4 Molar conductivity measurements

The conductivity Λ_m value of the La nanocomplexes **1–3** can be calculated by using the relation $\Lambda_m = K/C$. The complexes were (10^{-3} M) dissolved in DMF, and the molar conductivities of their solutions at $25\pm 2^\circ\text{C}$ were measured (**Table 1**). It is concluded from the results that complexes **1** and **3** are found to have molar conductance values of 20.51 and $3.39\text{ ohm}^{-1}\text{ mol}^{-1}\text{ cm}^2$, respectively, indicating that these complexes are nonelectrolytic and monomeric in nature. Also the values indicate the bonding of the nitrate ions to metal cations [28, 29]. The molar conductivity value of complex **2** is seen to be $57.88\text{ ohm}^{-1}\text{ mol}^{-1}\text{ cm}^2$ indicating the ionic nature of this complex, and the nitrate ion is outside the coordination sphere.

3.5 Electronic spectral data

The assignments of the significant electronic spectral absorption band of the nanometal complexes are given in Table 3. Two absorption peaks were observed in the spectra range of 210 – 227 and 279 – 337 nm due to $\pi\text{--}\pi^*$ and $n\text{--}\pi^*$ transitions, respectively, due to benzene and the azomethine (CH=N) function [26, 29]. Moreover, the spectra of complexes indicate no significant absorption in the visible region due to the absence of $f\text{--}f$ transition, since $f\text{--}f$ transitions are Laporte-forbidden and very weak in nature.

Compd. no.	μ_{eff} (B.M.)	Absorption bands (nm)	
		$\pi\text{-}\pi^*$	$n\text{-}\pi^*$
1	Diamagnetic	269	337
2	Diamagnetic	210	280
3	Diamagnetic	227	279

Table 3.

Magnetic moment and electronic spectral data of La(III) nanocomplexes.

3.6 Magnetic susceptibility

The following equation was used to calculate the magnetic susceptibility of the La nanocomplexes:

$$X_g = \frac{C(bal)(1)(R - R^0)}{10^{-9}\text{m}} \quad (1)$$

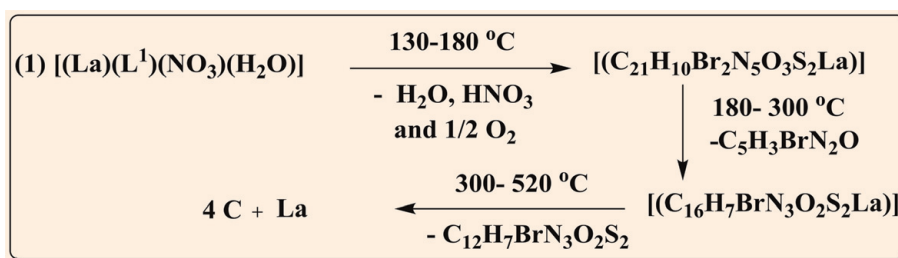
where C, calibration constant of standard; l, length of sample in filled tube; R^0 , reading of empty sample tube; R, reading with sample; χ_g gram magnetic susceptibility.

The gram magnetic susceptibility of the complexes was found in the range -2.2098×10^{-6} $-(-2.3013 \times 10^{-6}) \text{ cm}^3 \text{ mol}^{-1}$, respectively. Negative values of χ_g show that these complexes are diamagnetic in nature or there is no significant magnetic moment (**Table 3**).

3.7 Thermal analysis

Thermogravimetric analyses (TGA) of the La nanocomplexes were used to determine the thermal stability of the complexes, decide whether the water molecules are lattice or coordinated, and finally suggest a scheme for thermal decomposition of these chelates. In the present investigation, heating rates were suitably controlled at $10^\circ\text{C min}^{-1}$ under nitrogen atmosphere, and the weight loss was measured from the ambient temperature up to $\sim 600^\circ\text{C}$. The weight loss for each chelate was calculated within the corresponding temperature ranges.

Also, TGA curve of the La(III) complex of nanoscale $[(\text{La})(\text{L}^1)(\text{NO}_3)(\text{H}_2\text{O})]$ (**1**) showed three thermal stages. The first stage represents the loss of H_2O molecule of coordination, HNO_3 and $\frac{1}{2}\text{O}_2$ with a found weight loss of 11.72% (calcd. 11.54%) within the temperature range of $130\text{--}180^\circ\text{C}$; the subsequent second step ($180\text{--}300^\circ\text{C}$) corresponds to the loss of $\text{C}_5\text{H}_3\text{BrN}_2\text{O}$ with an estimated mass loss of 22.60% (calcd. 22.27%). The final stage at $300\text{--}520^\circ\text{C}$ corresponds to loss of rest of the organic part ($\text{C}_{12}\text{H}_7\text{BrN}_3\text{O}_2\text{S}_2$) with an estimated weight loss 44.25% (calcd. 43.94%) leaving 4 C and La metal as a metallic residue. The overall weight loss amounts is 78.57% (calcd. 77.75%):



3.8 Powder X-ray diffraction studies

The diffraction of X-rays from the planes of a crystal (diffraction analysis) is considered as one of the important methods of the analytical work. By using X-ray diffraction which depends on the crystal properties of solids, we can identify the crystal structure of various solid compounds and identify the actual compounds from its structure, and we can also determine the arrangement of molecules in crystal [30]. X-ray diffractometry is an important technique as it is a nondestructive, non-contrast, fast, and sensitive one. Obtained XRD data of H_2L^1 ligand and its La(III) complex **1** of nanoparticle (**Figure 2**) show that XRD pattern of the ligand is different in comparison with the XRD pattern of the nanocomplex. The obtained data indicate that the complex is more crystalline in nature than that of the ligand which has an amorphous phase. The average particle size of the complex (**1**) can be estimated from Debye-Scherrer equation (Eq. (2)):

$$L = K\lambda/\beta \cos\theta \quad (2)$$

where β the breadth of the observed diffraction line at its half intensity maximum; K , the shape factor, 0.89; λ , the wavelength of the X-ray source used in XRD; θ , the corresponding incidence angle.

The average particle size of the nanoparticles is 15 nm. The sharp diffraction peaks of the samples indicate that the well-crystallized lanthanum complex nanocrystals can be prepared by our procedure [23].

3.9 EDX spectra

The amount of elements present in the percentage level of the metal complexes was identified by EDX data [31]. EDX spectra are used to calculate the percentage level of the elements present in the metal complexes like C, O, N, S, and La that are present in the La(III) nanocomplex **2**, shown in **Figure 3**. The revealed data are in good agreement with that of the elemental analysis.

3.10 SEM analysis

SEM technique was used to study the morphology and size of nanoparticles (**Figure 4**). It seems that the particles are semispherical with some agglomerations

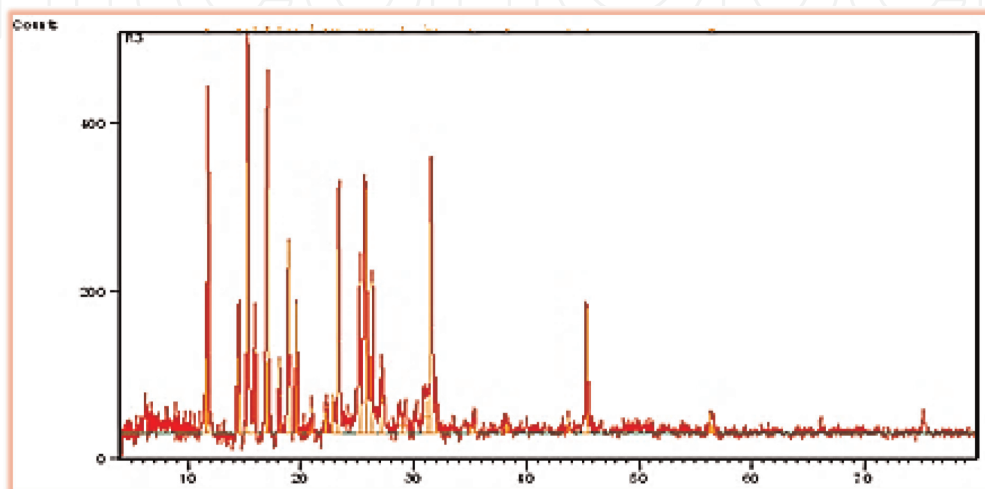


Figure 2.
X-ray powder diffractogram of complex (**1**) nanoparticle.

of the particles. The SEM images further revealed the stabilization of La(III) **1** nanoparticles due to interaction with the Schiff base ligand; this stabilization facilitates penetration of tumor cell membrane and causes the destruction of tumor cell [32].

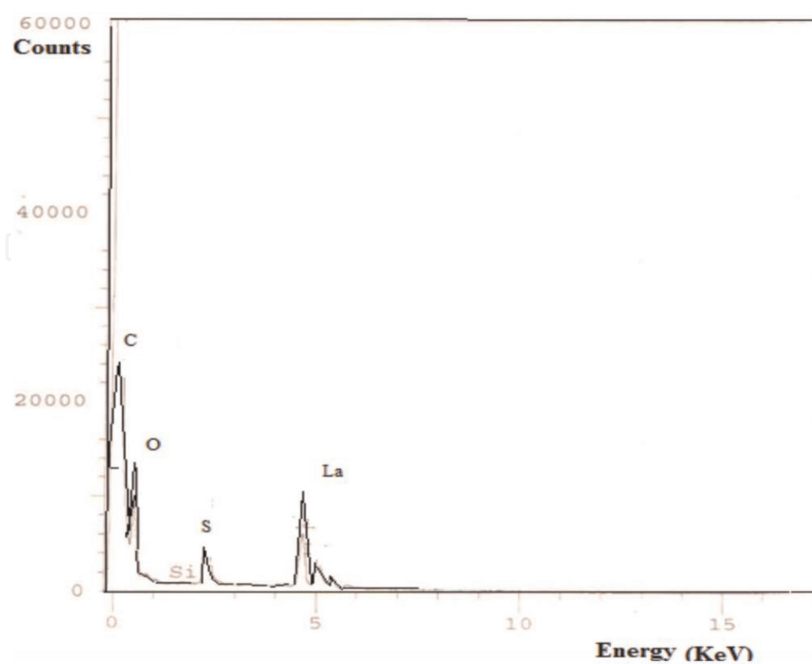


Figure 3.
EDX spectra of nano-La(III) complex 2.

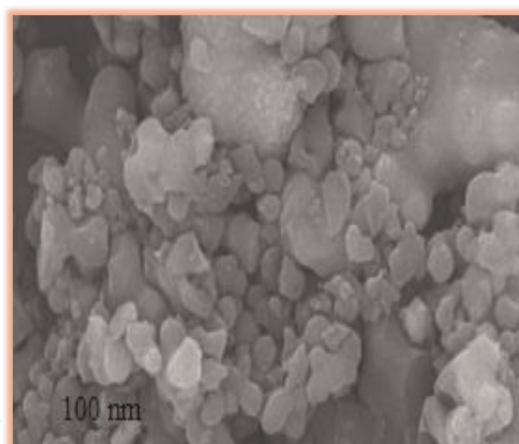


Figure 4.
SEM images of nanoparticles as produced by ultrasound $[(La)(L^1)(NO_3)(H_2O)]$ (**1**).

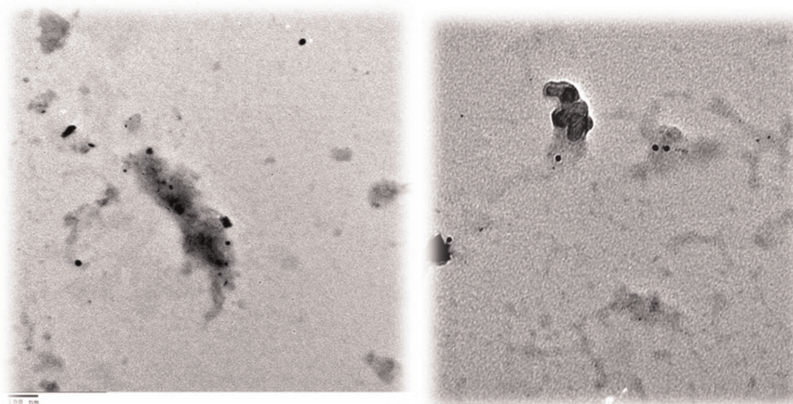


Figure 5.
TEM image of La(III) nanocomplex 2.

3.11 TEM analysis

Transmission electron microscopy (TEM) can be used to directly image nanoparticles at scales approaching a single atom. TEM analysis is performed to examine the size and shape of the nanoparticles. The La(III) complex 2 nanoparticle was fairly uniform in size, spherical in shape, and with the average diameter

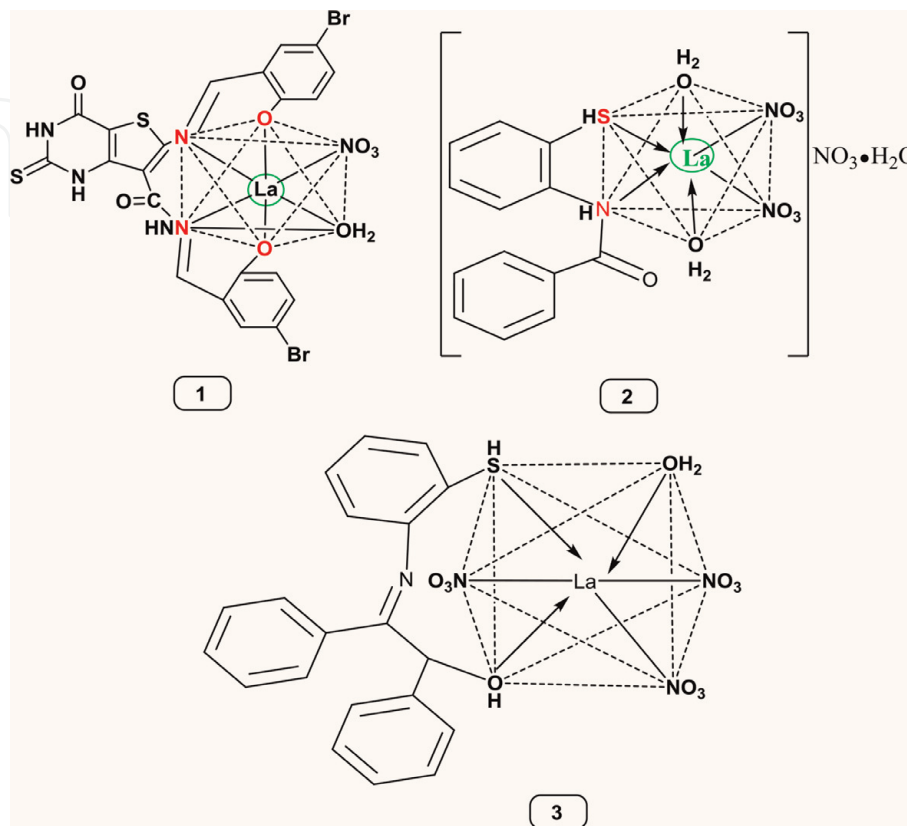


Figure 6.
Suggested structure of metal complexes 1–3.

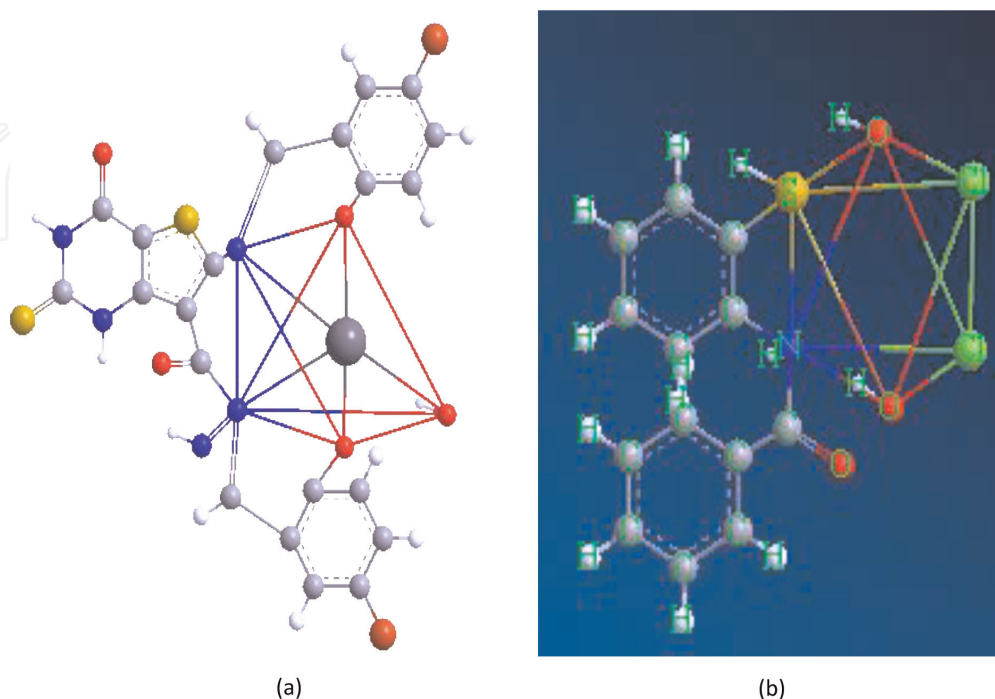


Figure 7.
Geometry-optimized structures of (a) complex 1 (b) La complex 2.

ranging from 3.2 to 44.9 nm (**Figure 5**). Electron microscopy analysis allowed confirming visually the observed stability of the obtained nanocomplex.

Correlation of all results obtained for the complexes under study gives us information regarding the suggested structure of the complexes to be as in **Figure 6**. The fully optimized geometries of the ligand and its metal complexes were shown in **Figure 7**.

4. Title

4.1 Cytotoxicity and anticancer activity

The cytotoxicity of the prepared nanocomplexes has been demonstrated and tested for their anticancer activity against Caco2, Vero, and MCF-7 cell lines. The obtained results revealed that complex **1** had the best recorded anticancer activity against Caco2 cells with inhibition percentage of 72.13 (**Figure 8B**). The IC_{50} (μg) (the value which corresponds to the concentration required for 50% inhibition cell viability) for the noncytotoxic doses against human primary dermal fibroblasts cells were recorded as 2.482 $\mu\text{g}/\text{ml}$. The IC_{50} for these structures were recorded as 0.3772 $\mu\text{g}/\text{ml}$ for compound **1** on Caco2 cells. In spite of the potency of the sample as anticancer agents, the superior selectivity index values against Caco2 cells than noncancerous cells were recorded with a value of 46.6.

On the other hand, the other tested compounds have shown moderate activities against all cells; the anticancer activity is less than that recorded for **1**.

4.2 Flow cytometry

Flow cytometric analyses of propidium iodide-stained nuclei cells were performed to investigate whether treatment could induce cell cycle perturbations in human epithelial colorectal adenocarcinoma. Cell cycle parameters were compared for Caco2 cells that had been incubated for 24 h with 1 ml of IC_{50} concentrations of sample **1** with untreated (control) cells. As shown in **Figure 9**, following 24 h incubation with treatment, there was an increase in the proportion of cells in the G2/M phase (51.10%, for treatment **1**).

Also, an additional peak was observed, consistent with aneuploid cells which contain more than $4n$ DNA. This peak may represent a population of cells that has escaped mitotic arrest and continued to replicate as multinuclear cells without dividing (i.e., endoreduplication), or it may be due to a small fraction of tetraploid

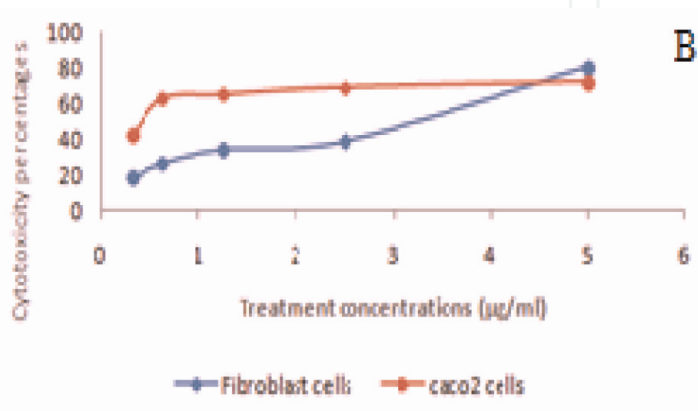


Figure 8.

Cytotoxicity and anticancer activity of the prepared compounds against human primary dermal fibroblasts and Caco2 cell lines, respectively.

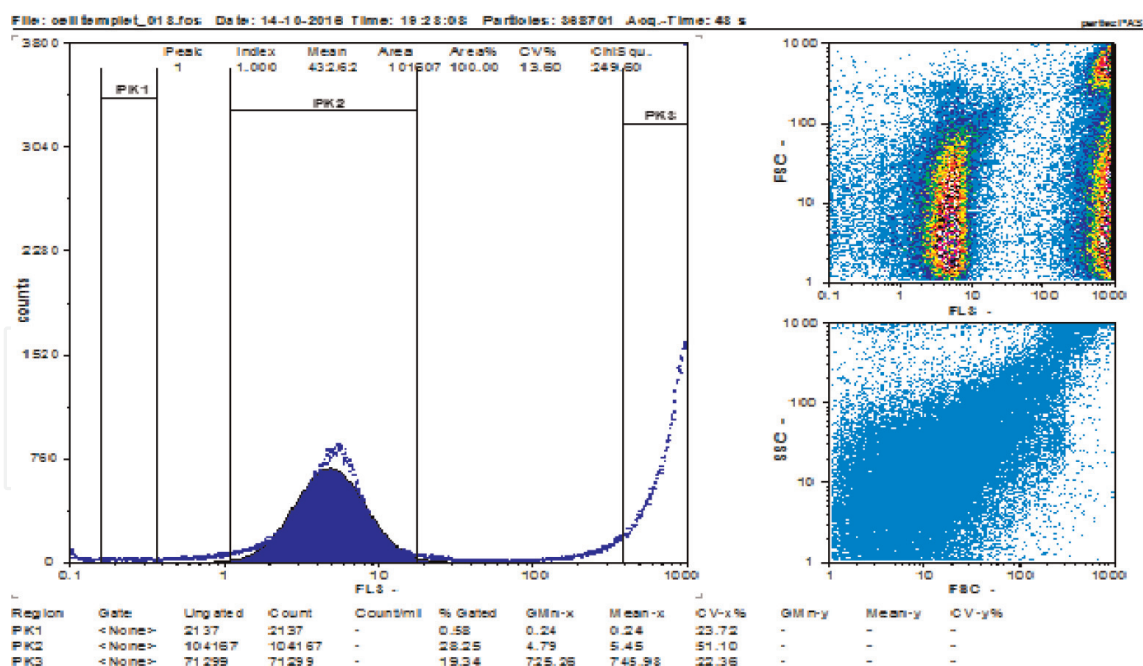


Figure 9.
 Flow cytometric analysis of compound 1, against Caco2 cell line.

cells which are already present in the culture, which undergo G2/M arrest, resulting in cells with 8n DNA.

4.3 Chitosan-nanocomplex 2 composite nanofibers

The chitosan played an important role in the synthesis of the composite nanofiber. The amino group has been used to stabilize metal nanoparticles [33], so we suggested that the free NH_2 ligands of chitosan might bind to the nanoparticles and stabilized them.

4.3.1 FTIR

The formation of the CS-stabilized NPs was further investigated by FTIR spectroscopy. The FTIR spectra of the CS-NP nanofiber and CS nanofiber attributed a broad band at the range of $3350\text{--}3510\text{ cm}^{-1}$ corresponding to the amine and hydroxyl groups. For the nanocomposite, there is a change in the shape and frequencies of the bands in this region, indicating participation of the NH_2 group in the reaction. Although there is some difference in the two figures, both of them showed the basic characteristic peaks for CS at 3422 cm^{-1} (O–H stretch) and $2960\text{--}2970\text{ cm}^{-1}$ (C–H stretch), which indicated that the CS can adsorb on the formed nanoparticles in the preparation process [34, 35].

4.3.2 TGA

Thermogravimetric analysis (TGA) is widely used to investigate the thermal decomposition of a polymer. The TGA thermograms of pristine CS nanofiber, CS-NP composite nanofiber, at a heating rate of $20^\circ\text{C}/\text{min}$ under nitrogen atmosphere are investigated. Chitosan's nanofiber weight change between 28.27 and 100°C is associated with the loss of adsorbed and bound water. Chitosan polymer degradation started at 100°C and continued up to 333.80°C , with a 75.5% polymer weight loss [36, 37].

The CS-NP composite nanofiber exhibited a three-step degradation pattern. The first step occurred between 24.68°C and 100.86°C, which is due to water evaporation. The second and the major mass loss were observed between 100°C and 261.34°C, with a 40.42% polymer weight loss. The third step occurred between 261.34 and 367.43°C, with a 19.95% polymer weight loss with total loss of 71.27% at 367.43°C.

4.3.3 TEM

The NP complex was encapsulated by CS, and their sizes were in the range of 15–50 nm as shown in the TEM image of the CS–NP composite nanofiber (**Figure 10**). It could be observed that a considerable amount of non-spherical particle was observed. These non-spherical particles seemed to be fabricated by coalescence of two spherical particles during the nucleation process [38].

4.3.4 SEM

The morphology of electrospun (chitosan–nanoparticle) composite nanofiber is shown in **Figure 11**. It is clear from these figures that no phase separation has been observed and the homogeneity of the obtained nanofibers can be easily observed and the composite of the nanoparticles has been proven. It is also clear that the diameter of chitosan–nanoparticle composite nanofiber is smaller than chitosan nanofiber.

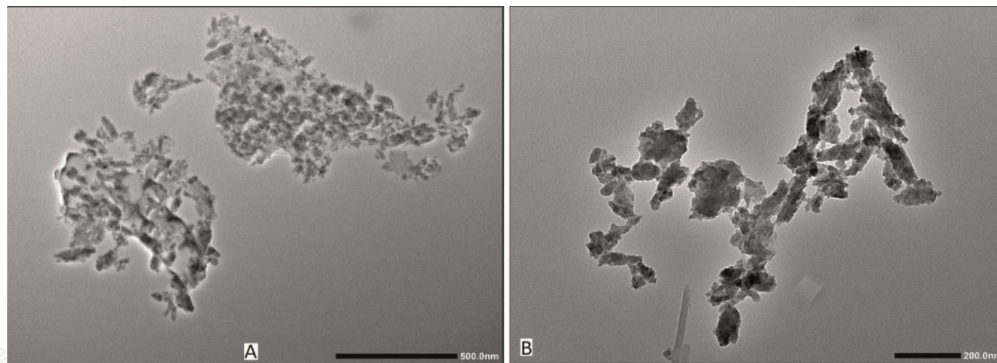


Figure 10.
TEM micrograph of (A) chitosan nanofiber and (B) (chitosan-nanoparticle) composite nanofiber.

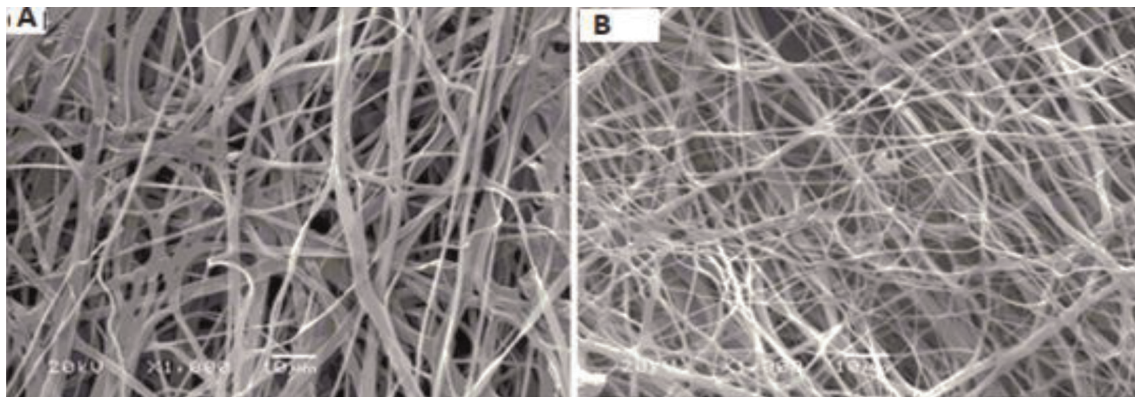


Figure 11.
SEM micrograph 1000× of (A) CS nanofiber and (B) La-CS composite nanofiber.

4.3.5 Antimicrobial activity

The ability of prepared La nanoparticle-coated nanofibers to cease the growth of microbes known for its human pathogenicity has been investigated. La nanoparticle-coated nanofibers succeeded to locally cease the growth of all tested microbes. Each disc succeeded to stop the growth of tested microbes at the boundaries between the disc and the plates' surfaces, forming clear zones with 7 mm diameter. It is worth mentioning that La nanoparticle-coated nanofibers showed the same pattern of antimicrobial activity against all tested microbes. The ability of prepared nanoparticle-nanofiber hybrid to affect the microbes locally is definitely promising for biomedical applications. These results would support the coexistence of the microbes and their antimicrobial agent at the same location and hence improve the overall microbe drug interaction process. Moreover, this kind of antimicrobial agent localization would prevent the probability of its migration to other sites inside the body that would help to avoid the expected subsidiary complications. It would be recommended that these nanoparticle-coated nanofibers are used as wound dressing for skin injuries.

5. Conclusion

La(III) nanocomplexes with different organic ligands were synthesized and characterized by different techniques. In addition to the nanosize was proved by different techniques also. All prepared metal complexes were screened against different human cell lines. It was found that we were able to identify new potent and selective anticancer compounds. Also, one of these nanocomplexes was tested as wound dressing which is recommended to be used as local chemotherapy for skin injuries.

Author details


Rania H. Taha^{1,2}

1 Chemistry Department, College of Science, Jouf University, Sakaka, Saudi Arabia

2 Department of Chemistry, Faculty of Science (Girls), Al-Azhar University, Nasr City, Cairo, Egypt

*Address all correspondence to: mhmd_mosad@yahoo.com; rania@azhar.edu.eg

IntechOpen

© 2019 The Author(s). Licensee IntechOpen. This chapter is distributed under the terms of the Creative Commons Attribution License (<http://creativecommons.org/licenses/by/3.0>), which permits unrestricted use, distribution, and reproduction in any medium, provided the original work is properly cited. 

References

- [1] Dunn PJ. The importance of green chemistry in process research and development. *Chemical Society Reviews*. 2012;**41**:1452-1461
- [2] Gou Y, Li J, Fan B, Xu B, Zhou M, Yang F. Structure and biological properties of mixed-ligand Cu(II) Schiff base complexes as potential anticancer agents. *European Journal of Medicinal Chemistry*. 2017;**134**:207-217
- [3] Binil PS, Anoop MR, Jisha KR, Suma S, Sudarsanakumar MR. Synthesis, spectral characterization, thermal and biological studies of lanthanide(III) complexes of oxyphenbutazone. *Journal of Rare Earths*. 2014;**32**:43
- [4] Bouchoucha A, Terbouche A, Bourouina A, Djebbar S. New complexes of manganese (II), nickel (II) and copper (II) with derived benzoxazole ligands: Synthesis, characterization, DFT, antimicrobial activity, acute and subacute toxicity. *Inorganica Chimica Acta*. 2014;**418**:187
- [5] Saad FA, El-Metwaly NM, Farghaly TA, Elghalban MG, Shah RK, Al-Hazmid GA, et al. Illustration for series of new metal ion complexes extracted from pyrazolone derivative, spectral, thermal, QSAR, DFT/B3LYP, docking and antitumor investigations. *Journal of Molecular Liquids*. 2017;**229**:614
- [6] Delgado S, Santana A, Castillo O, Zamoro F. Dynamic combinatorial chemistry in a solvothermal process of Cu(I,II) and organosulfur ligands. *Dalton Transactions*. 2010;**39**:2280
- [7] Hsu H-Y, Tseng C-C, Chung-Ming Sun BM. Ionic liquid-supported synthesis of dihydroquinazolines and tetrahydroquinazolines under microwave irradiation. *Molecular Diversity*. 2012;**16**:241
- [8] Baghbanzadeh M, Pilger C, Kappe CO. Rapid nickel-catalyzed Suzuki-miyaura cross-couplings of aryl carbamates and sulfamates utilizing microwave heating. *The Journal of Organic Chemistry*. 2011;**76**:1507
- [9] Qin W, Long S, Panunzio M, Biondi S. Schiff bases: A short survey on an evergreen chemistry tool. *Molecules*. 2013;**18**:12264
- [10] Manju N, Mishra D, Kumar R. Coordination chemistry of Schiff base tin complexes. *Journal of Coordination Chemistry*. 2014;**40**:343
- [11] Evans CH. *Biochemistry of the Lanthanides, Lanthanides Series Determination by Various Analytical Methods*. New York & London: Plenum Press; 1990
- [12] Biba F, Groessl M, Egger A, Roller A, Hartinger CG, Keppler BK. New insights into the chemistry of the antineoplastic lanthanum complex tris (1,10-phenanthroline)tris (thiocyanato- κ N)lanthanum(III) (KP772) and its interaction with biomolecules. *European Journal of Inorganic Chemistry*. 2009;**2009**:4282
- [13] Kostova I, Momekov G, Zaharieva M, Karaivanova M. Cytotoxic activity of new lanthanum (III) complexes of bis-coumarins. *European Journal of Medicinal Chemistry*. 2005;**40**:542
- [14] Kostova I, Momekov G. New cerium (III) complexes of coumarins—Synthesis, characterization and cytotoxicity evaluation. *European Journal of Medicinal Chemistry*. 2008;**43**:178
- [15] Kulkarni A, Patil SA, Badami PS. Synthesis, characterization, DNA cleavage and in vitro antimicrobial studies of La(III), Th(IV) and VO(IV)

complexes with Schiff bases of coumarin derivatives. *European Journal of Medicinal Chemistry*. 2009;**44**:2904

[16] Chen JG, Qiao X, Gao YC, et al. Synthesis, DNA binding, photo-induced DNA cleavage and cell cytotoxicity studies of a family of light rare earth complexes. *Journal of Inorganic Biochemistry*. 2012;**109**:90

[17] Mogosanu GD, Grumezescu AM. Natural and synthetic polymers for wounds and burns dressing. *International Journal of Pharmaceutics*. 2014;**463**:127-136

[18] Sedghi R, Shaabani A, Mohammadi Z, Yazdi F, Isaei E. Carbohydrate Polymers. 2017;**159**:1-10

[19] Almahdy O, EL-Fakharany EM, EL-Dabaa E, Ng TB, Redwan EM. Examination of the activity of camel milk casein against hepatitis C virus (genotype-4a) and its apoptotic potential in hepatoma and HeLa cell lines. *Hepatitis Monthly*. 2011;**11**: 724-730

[20] El-Fakharany EM, Sánchez L, Al-Mehdar HA, Redwan EM. Effectiveness of human, camel, bovine and sheep lactoferrin on the hepatitis C virus cellular infectivity: Comparison study. *Virology Journal*. 2013;**10**:199

[21] Mosmann T. Rapid colorimetric assay for cellular growth and survival: Application to proliferation and cytotoxicity assays. *Journal of Immunological Methods*. 1983;**65**:55-63

[22] Léonce S, Perez V, Lambel S, Peyroulan D, Tillequin F, Michel S, et al. Induction of cyclin E and inhibition of DNA synthesis by the novel acronycine derivative S23906-1 precede the irreversible arrest of tumor cells in S phase leading to apoptosis. *Molecular Pharmacology*. 2001;**60**:1383-1391

[23] Aly HM, Taha RH, El-Deeb NM, Alshehri A. Efficient procedure with new fused pyrimidinone derivatives, Schiff base ligand and its La and Gd complexes by green chemistry. *Inorganic Chemistry Frontiers*. 2018;**5**: 454-473

[24] Fasina MT, Ogundele OO, Ayeni I. Synthesis and biological properties of N₂O₂ Schiff bases derived from o-phenylenediamine and substituted salicylaldehydes. *Journal of Chemical and Pharmaceutical Research*. 2014;**6**: 816-819

[25] Gomathi V, Selvameena R. Synthesis, spectroscopic, electrochemical and biological studies of Schiff base complexes of some 3d transition metals derived from 2-aminophenol and 2-hydroxynaphthaldehyde. *Indian Journal of Applied Research*. 2013;**3**(4):51-53

[26] Rania HT. Preparation. Spectroscopic Characterization, DNA Cleavage, Antimicrobial and Antitumor Investigations of Nickel and Uranyl Schiff Base Complexes in Bulk and Nano size. *Current Science International*. 2015; **4**(4):684-700

[27] Khandelwal A, Agrawal M, Lamba S, Baswal G. Synthesis and characterization of mixed ligand complexes of Mn(III) with 5-bromosalicylaldehyde and 2-hydroxyaryl carbonyl compounds or β -diketones. *Weekly Science Research Journal*. 2013;**1**:1-10

[28] Rania HT, Zienab AE, Aida AS, Esmail ME, Mai MM. Synthesis and characterization of newly synthesized Schiff base ligand and its metal complexes as potent anticancer. *Journal of Molecular Structure*. 2019;**1181**:536-545

[29] Mohebbi S, Bakhshi B. Electrochemical and spectral behavior

of mononuclear oxovanadium(IV) salicyldiimine complexes. *Journal of Coordination Chemistry*. 2008;**61**:2615

[30] Podorov SG, Faleev NN, Pavlov KM, Paganin DM, Stepanov SA, Forster E. New approach to wide-angle dynamical X-ray diffraction by deformed crystals. *Journal of Applied Crystallography*. 2006;**39**:652

[31] Soheir SA, Rania HT, Amany MT, Mohamed OA, Hanady AM. Antimicrobial activity of bio and chemical synthesized cadmium sulfide nanoparticles. *The Egyptian Journal of Hospital Medicine*. 2018;**70**(9):1494-1507

[32] Mandegani Z, Mozaffar A, Zahra A, Afshan M, Nasser I, Akbar O. A nano tetraimine Pd(0) complex: Synthesis, characterization, computational studies and catalytic applications in the Heck–Mizoroki reaction in water. *Green Chemistry*. 2015;**17**:3326-3337

[33] Selvakannan PR, Mandal S, Phadtare S, Pasricha R, Sastry M. *Langmuir*. 2003;**19**:3545-3549

[34] Kumar CV, McLendon GL. *Chemistry of Materials*. 1997;**9**:863-870

[35] He P, Hu N, Rusling JF. *Langmuir*. 2004;**20**:722-729

[36] Rosi M, IskandarAbdullah F, Khairurrijal M. Hydrogel-polymerelectrolytes based on polyvinyl alcohol and hydroxyethylcellulose for supercapacitor applications. *International Journal of Electrochemical Science*. 2014;**9**(8):4251-4256

[37] Abu-Saied MA, Wycisk R, Abbassy MM, El-Naim GA, El-Demerdash F, Youssef ME, et al. Sulfated chitosan/PVA absorbent membrane for removal of copper and nickel ions from aqueous solutions—Fabrication and sorption studies. *Carbohydrate Polymers*. 2017;**165**(1):149-158

[38] Bharathi S, Fishelson N, Lev O. *Langmuir*. 1999;**15**:1929-1937

[39] Abu-Saied MA, Khalil KA, Al-Deyab SS. Preparation and characterization of poly vinyl acetate nanofiber doping copper metal. *International Journal of Electrochemical Science*. 2012;**7**: 2019-2027